

Hole Spin Resonance and Spin-Orbit Coupling in a Silicon Metal-Oxide-Semiconductor Field-Effect Transistor

K. Ono,^{1,*} G. Giavaras,² T. Tanamoto,³ T. Ohguro,³ X. Hu,^{2,4} and F. Nori^{2,5}

¹*Advanced device laboratory, RIKEN, Wako-shi, Saitama 351-0198, Japan*

²*CEMS, RIKEN, Wako-shi, Saitama 351-0198, Japan*

³*Corporate R&D Center, Toshiba Corporation, Kawasaki-shi, Kanagawa 212-8582, Japan*

⁴*Department of Physics, University at Buffalo, SUNY, Buffalo, New York 14260-1500, USA*

⁵*Department of Physics, The University of Michigan, Ann Arbor, Michigan 48109-1040, USA*

(Received 29 March 2017; revised manuscript received 14 June 2017; published 11 October 2017)

We study hole spin resonance in a *p*-channel silicon metal-oxide-semiconductor field-effect transistor. In the subthreshold region, the measured source-drain current reveals a double dot in the channel. The observed spin resonance spectra agree with a model of strongly coupled two-spin states in the presence of a spin-orbit-induced anticrossing. Detailed spectroscopy at the anticrossing shows a suppressed spin resonance signal due to spin-orbit-induced quantum state mixing. This suppression is also observed for multiphoton spin resonances. Our experimental observations agree with theoretical calculations.

DOI: [10.1103/PhysRevLett.119.156802](https://doi.org/10.1103/PhysRevLett.119.156802)

The silicon-based metal-oxide-semiconductor field-effect transistor (MOSFET) is a key element of large-scale integrated circuits that are at the core of modern technology. Looking into the future, a universal fault-tolerant quantum computer also requires a huge number of physical qubits, on the order of 10^8 or more [1,2]. As such, a qubit integrated with the standard Si MOSFET architecture would be truly attractive from the perspectives of scaling up and leveraging existing technologies. One example of such a qubit is the spin of an impurity or defect in the channel of a Si MOSFET. Indeed, spin qubits defined in Si nanodevices are not only compatible with current silicon technology, but are also known to be one of the most quantum coherent among qubit designs [3–14].

There are many studies of impurities and defects in Si [15–17]. The single impurity or defect in the channel of a Si MOSFET has been studied by the telegraph switching of an on-state current [18], and more recently by single electron tunneling [19–23]. Spins of such defects are difficult to characterize because of their weakly interacting nature. Controlling the spins of impurities in a MOSFET, as well as in a gate-confined quantum dot, can be achieved much more easily in a *p*-channel than an *n*-channel MOSFET. The reason is that the larger spin-orbit interaction (SOI) of a hole (-like) spin enables the spin resonance by an oscillatory electric field, instead of a magnetic field, at microwave frequencies under typical sub-Tesla static magnetic fields. Such electrically driven spin resonance (EDSR) has been demonstrated in III-V devices [24–27], as well as in Si [28–30]. However, systematic investigations of EDSR under the direct influence of SOI have not been performed in Si, the material that provides an ideal stage for studying SOI due to the minor presence of nuclear spins.

In this Letter, we study subthreshold transport and EDSR in a short *p*-channel Si MOSFET, and quantitatively reveal the effects of SOI and EDSR on lifting the spin blockade. Specifically, our transport measurements demonstrate that there are two effective dots in the channel which allow us to identify a spin blockade regime and explore spin resonance for two strongly coupled holes. The observed two-spin EDSR spectra, in particular, the magnetic field dependence of the resonances and the associated state mixing, provide clear evidence of a SOI-induced anticrossing with a well-resolved spin-orbit gap. Spectroscopy near the anticrossing shows a suppressed EDSR signal because the involved states are almost equally populated as a result of the maximum SOI-induced state mixing. Our observations of spin blockade, single as well as multiphoton spin resonance, and spin-orbit-induced state mixing are important steps toward the precise control of spin qubits in Si MOSFETs.

Our device is a *p*-channel MOSFET with a channel length of 135 nm and width of 220 nm, as shown in Fig. 1(a). It has a silicon-oxynitride gate dielectric and is fabricated with standard $0.13\ \mu\text{m}$ CMOS technology. The measurements are performed in a ^4He pumped cryostat at a temperature of $T = 1.6$ K. A magnetic field is applied parallel to the MOS interface and the source-drain current, and a microwave (MW) field is applied directly to the gate electrode. Figure 1(c) shows the measured current in the subthreshold region. Specifically, we measure the source-drain differential conductance as we vary the source-drain (V_S) and gate (V_G) voltages. A Coulomb diamond with charging energy of 25 meV is observed centered around $V_G = -0.62$ V. The current in this diamond is about 3 orders of magnitude smaller than the on-state current of the MOSFET, which is a clear evidence of Coulomb blockade.

This has been observed in MOSFETs before and attributed to sequential tunneling through a single dopant or defect in the channel [19–23].

An important feature of Fig. 1(c), however, is that the Coulomb diamond around $V_G = -0.62$ V does not close all the way to $V_S = 0$ at both its ends near $V_G = -0.60$ V and $V_G = -0.63$ V (this is particularly clear near $V_G = -0.60$ V). This indicates the presence of a larger dot that is detuned from and coupled in series with a more tightly confined dot, so that sequential tunneling through the double quantum dot (DQD) can only take place at finite source-drain bias. The data in Fig. 1(c) indicate that the two dots have a weak (~ 5 meV) and a strong (~ 25 meV) confinement. The strongly confined dot could be a Boron dopant in the channel or a dangling bond defect at the silicon-oxynitride interface, whereas the weakly confined dot could arise from potential fluctuations caused by remote impurities or defects. The physical system can then be represented schematically as shown in Fig. 1(b). Thermal cycles between 1.6 and 300 K slightly shift the gate voltage dependence, but the Coulomb diamond and the microwave spectroscopy data remain the same after the cycles, indicating the robustness of the double dot.

An interesting regime of double quantum dots is the spin blockade regime, where spin symmetries are correlated with charge configurations [31–33]. In our double dot device, we have evidence of spin blockade. Recall that, in the spin blockade [31], transport is blocked if the two-spin state is one of the triplet states, T_- , T_0 , or T_+ . Lifting the spin blockade requires cotunneling and/or spin relaxation to the singlet state S that consists of S_{11} and S_{02} components [34]. Specifically, in the area enclosed by the dotted curve in Fig. 1(c), the current is suppressed outside the Coulomb blockade diamond, which indicates that details of the electronic states, such as spin symmetry, prevent holes from sequential tunneling. Further evidence of spin blockade is revealed when the suppression of conduction is lifted by a microwave applied to the gate electrode, and well-defined current peaks appear depending on both the external magnetic field and the microwave frequency [Fig. 1(e)]. These microwave-induced peaks define the high-current curves seen in Fig. 1(e), and are due to spin excitations that lift the spin blockade which was originally in place. No EDSR was observed on the opposite side of the Coulomb diamond, for $V_S < 0$, mostly because the tunneling is asymmetric for a MOSFET that is forward and reverse biased.

The spectroscopic features of Fig. 1(e) can be qualitatively explained by the low-energy spectrum of two-hole spin states in a double dot [Fig. 1(d)] and also dovetail nicely with the picture of current suppression due to spin blockade. In our double dot, there is a singlet-triplet exchange splitting at zero magnetic field due to mixing between the S_{11} and S_{02} singlets [34]. When a finite magnetic field is applied, the triplet states Zeeman split,

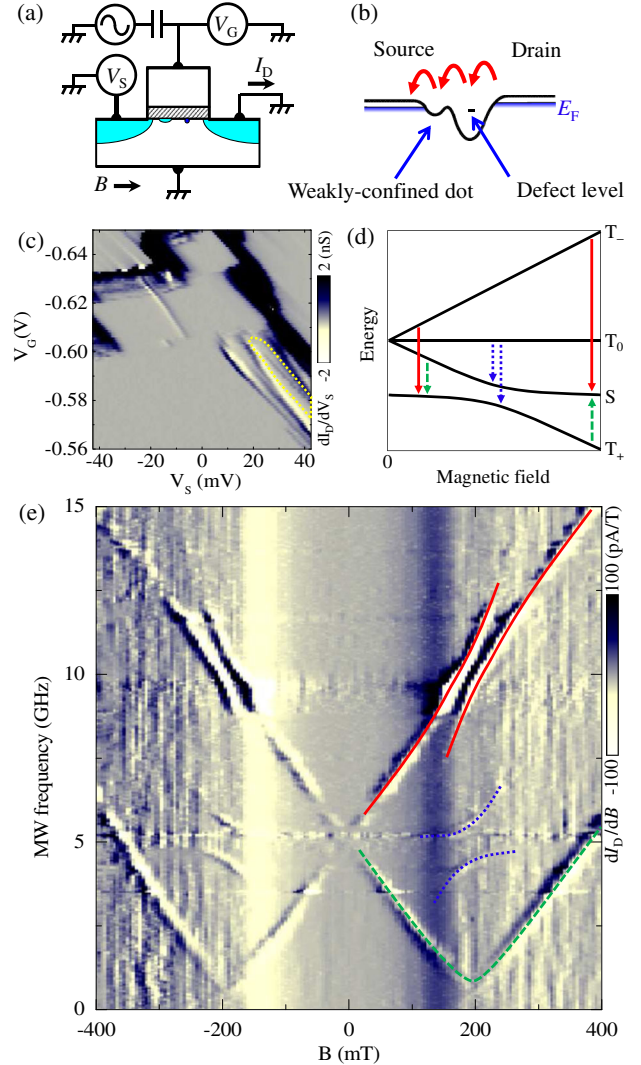


FIG. 1. (a) Schematic of the MOSFET device and measurement setup. (b) Potential landscape of quantum dots. (c) Intensity plot of dI_D/dV_S near the subthreshold region. The spin resonance is observed in the region enclosed by the yellow dotted curve. The $dI_D/dV_S = 0$ regions for $V_G \approx -0.635$ V are artifacts of the current meter. (d) Schematic energy diagram for two-hole states with a T_+-S anticrossing due to the spin-orbit interaction. The microwave-induced transitions T_+-S (red solid lines), T_0-S (blue dotted lines), T_+-S (green dashed lines) are indicated by vertical arrows. (e) Intensity plot of dI_D/dB measured at $V_S = 25$ mV, $V_G = -0.597$ V. For $B > 0$ the high-current EDSR curves due to the transitions T_+-S (red solid lines), T_0-S (blue dotted lines), T_+-S (green dashed lines) are indicated. Plotting dI_D/dB suppresses resonances at constant frequency due to photon-assisted tunneling enhanced by cavity modes.

with one of the polarized triplets eventually crossing the singlet state. The SOI couples the T_+ triplet with the S_{02} singlet and turns the crossing point into an anticrossing. The magnitude of the anticrossing gap is determined by the SOI matrix element between the T_+ and the S_{02} , and in our device it is about 1 GHz. The two eigenstates near the

anticrossing are mostly mixtures of S_{11} and S_{02} singlets together with the T_+ triplet. The field at which the anticrossing occurs, i.e., ± 200 mT in Fig. 1(e), is determined by the zero-field exchange splitting and the g factors in the two dots.

The high-current curves in Fig. 1(e) can now be attributed to microwave-induced transitions between the mixed singlet-triplet states as indicated by the arrows in Fig. 1(d). Microwave-induced transitions among the triplet states (T_{\pm} to T_0 , i.e., the normal EDSR transitions) do not lift the spin blockade and, thus, cannot be observed in our transport experiment. SOI does not couple T_0 and S states; thus, we do not observe a horizontal current curve in Fig. 1(e), except near the anticrossing, where the T_0 to T_+ transition is allowed and the spin blockade can be lifted because of the T_+-S mixing. Similar EDSR curves have also been observed in III-V nanowire double dots [26]. Notice that, in Fig. 1(e), the background current increases at ± 200 mT, independent of the microwave frequency, giving a clear vertical contrast at these fields. This increase is consistent with the enhanced scattering rate due to the SOI-induced $T_{\pm}-S$ mixing.

The EDSR spectra up to 40 GHz indicate that the g -factor difference between the two dots is small compared with the zero-field singlet-triplet splitting of about 5 GHz [35]. The slope of the current curves in Fig. 1(d) gives an average g factor for the two dots of 1.80. This is much larger than the value 1.1 observed for Boron dopants in bulk Si [48], while smaller than the value 2.0 of the dangling bond defect centers at the silicon-oxynitride interface [49]. Generally, we expect shallower defects to be more affected by the spin-orbit nature of the valence band, and their g factors should be smaller than the value of deep dangling bond defects. EDSR spectra, as in Fig. 1(e), can be observed throughout the spin blockade area enclosed by the dotted curve in Fig. 1(c). The g factor does not change significantly in this area, while the exchange energy can change by a factor of 2 depending on V_G . The typical linewidth of EDSR is 0.18 GHz, probably limited by the electrical charge noise due to the strong SOI in our device. We expect only a minor contribution of the nuclear spins to the EDSR linewidth due to the small content (4%) of ^{29}Si , and the p -orbital nature of holes.

Here we emphasize that our experiment is performed at a temperature of 1.6 K, which is over an order of magnitude higher than the usual temperatures of 0.1 K reported in previous works [20–26]. Performing the experiment at this high temperature is achieved thanks to the large orbital quantization energy of our dots. This also gives tolerance against unwanted photon-assisted tunneling or pumping current under strong driving.

For a more precise understanding of our observations, we focus on the T_+-S transition near the anticrossing point. This anticrossing has never been observed before, neither in

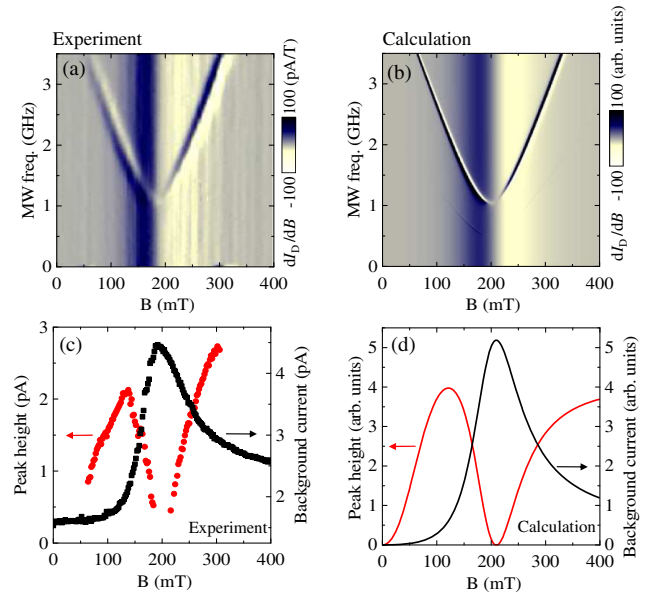


FIG. 2. (a) Measured and (b) calculated spin resonance spectra near the T_+-S anticrossing point for weak microwave driving [-40 dBm at the output of the microwave source for (a), and microwave amplitude $A = 30 \mu\text{eV}$ for (b)]. Measured (c) and calculated (d) peak height (bright line, left axis), and background current without microwave (dark line, right axis).

Si nor in III-V quantum dots. Figure 2(a) shows the leakage current (dI_D/dB) as a function of the microwave frequency and the magnetic field. The physics here can be well explained by a two-level model described in Ref. [35]. In brief, we incorporate the microwave driving by assuming that an electric field of amplitude A and frequency $f = \omega/2\pi$ modulates the on-site energy ε_2 of dot 2 periodically, namely, $\varepsilon_2 \rightarrow \varepsilon_2 + A \cos(\omega t)$. In other words, the transitions we study are purely electrically driven. The model considers the two energy levels E_1 and E_2 which anticross. The corresponding eigenstates are $|u_i\rangle = a_i|S_{11}\rangle + b_i|T_+\rangle + c_i|S_{02}\rangle + d_i|T_-\rangle$, $i = 1, 2$. The double dot parameters for $A = 0$ are chosen so that the levels anticross at about 200 mT, with a spin-orbit gap of about 1 GHz. The coefficients a_i , b_i , c_i , and d_i are obtained by diagonalizing the double dot Hamiltonian in the absence of the microwave. When the microwave is turned on, we perform a unitary transformation into a rotating frame [35], and within a rotating wave approximation, we obtain an approximate time-independent Hamiltonian for the single-photon spin resonance

$$h_{\text{DQD}} = \begin{pmatrix} E_1 + \hbar\omega/2 & q \\ q & E_2 - \hbar\omega/2 \end{pmatrix}, \quad (1)$$

with

$$q = \hbar\omega \frac{c_1 c_2}{(c_1^2 - c_2^2)} J_1 \left(\frac{A(c_1^2 - c_2^2)}{\hbar\omega} \right), \quad (2)$$

where J_1 is the 1st order Bessel function of the first kind [35]. We then calculate the current with a density matrix approach [35].

The theoretical results from this two-level model, shown in Fig. 2(b), are in good qualitative agreement with the experimental observations in Fig. 2(a). There are two important features common to both figures, one being the broad peak in the background current ($A = 0$) centered at about 200 mT independent of the microwave frequency. This peak is the result of the SOI-induced singlet-triplet mixing. It has an asymmetric form [36], unlike the usual symmetric line shape in a two-level system. The other common feature of Figs. 2(a) and 2(b) is the high-current curve due to the microwave-induced $T_+ \rightarrow S$ transition. The shape of this curve is hyperbolic, which arises from the normal anticrossing of two straight lines. The two-level model we adopt here gives us a good qualitative description of the experimental observations. We do not attempt to achieve quantitative agreement because of the missing information with regard to the device, such as the exact interdot tunnel coupling and the microscopic spin-orbit coupling mechanism. For example, differences in the EDSR linewidths between experiment and theory are most probably due to different cotunneling rates that limit the lifetime of spin states in the dots as well as additional decoherence sources that are not accounted for in the model.

Experimental data in Fig. 2(c) demonstrate that near the anticrossing at 200 mT the background current reaches a maximum, while the EDSR-induced current has a minimum. This minimum occurs even though the transition rate between the two levels due to the microwave field is the highest because of the maximized singlet-triplet mixing. This interesting feature can be understood within the two-level model. Recall that the leakage current in the spin blockade is due to mixing of the triplet with the singlet state. The microwave field, indeed, tends to equalize the occupations of the two levels, but near the anticrossing, the SOI already generates the maximum possible singlet-triplet mixing, so that transport of the holes occupying the T_+ triplet state is no longer blocked. This leads to a maximum in the leakage current, and transitions between the two states due to the microwave field cannot increase the current further. The effect of the microwave is therefore almost completely suppressed. This situation is similar to the well-known saturation of absorption under strong driving in spin resonance experiments [50], where the microwave equalizes the populations of the two levels and eventually leads to a decrease in the resonance signal. Figure 2(d) shows the calculated single-photon EDSR-induced current peak height as well as the background current, which are in nice qualitative agreement with the experimental observations in Fig. 2(c). Notice that, while at the $T_+ \rightarrow S$ anticrossing, the microwave-induced $T_+ \rightarrow S$ transition does not lead to further increase in current, the $T_0 \rightarrow S$ and $T_- \rightarrow S$ transitions do lead to a current increase

because they lift the spin blockade for holes occupying the T_- and T_0 states. In Fig. 1(c), the microwave-induced current increase is visible even at ± 200 mT.

In Fig. 2, the EDSR-induced current peaks also diminish for $B \rightarrow 0$ [the feature is also apparent in Fig. 1(e)]. Within the two-level model, when $B \rightarrow 0$, the state $|u_2\rangle$ becomes more exclusively the polarized triplet state, $|u_2\rangle \approx |T_+\rangle$, so that the coupling term $q \rightarrow 0$ because $c_2 \rightarrow 0$. Thus, the microwave field becomes less efficient in inducing direct transitions from any of the triplet states to the singlet, and the current peaks start to diminish for $B \rightarrow 0$. A cautionary note here, however, is that the two-level model becomes increasingly inaccurate as $B \rightarrow 0$. In this limit, the triplets become quasidegenerate. In the Supplemental Material [35], we discuss a more accurate calculation based on a Floquet master equation, which confirms the trends observed in Fig. 2.

Multiphoton EDSR has been observed before in double dots at strong microwave driving [51,52], away from the $T_+ \rightarrow S$ anticrossing. As shown in Figs. 3(a), 3(c), and 3(e), when we increase the microwave power in our device, we can generate additional current peaks. These peaks correspond to $n = 2, 3$, or more photons inducing transitions between the two levels that anticross. The resulting

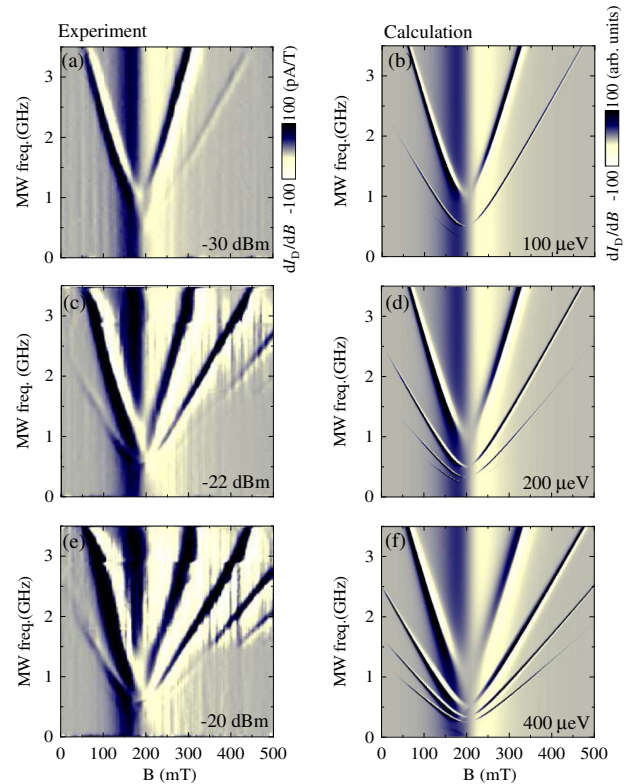


FIG. 3. Measured spin resonance spectra near the $T_+ \rightarrow S$ anticrossing at higher microwave powers (a) -30 dBm, (c) -22 dBm, and (e) -20 dBm at the output of the microwave source, respectively. Results of calculation for microwave amplitude (b) $A = 100 \mu\text{eV}$, (d) $A = 200 \mu\text{eV}$, and (f) $A = 400 \mu\text{eV}$.

multiphoton high-current curves are extrapolated to the $1/n$ of the spin-orbit gap at 200 mT. The multiphoton peaks can be reproduced with the two-level model discussed above when we use the appropriate n -photon Hamiltonian [35]. The theoretical results in Figs. 3(b), 3(d), and 3(f) are in good qualitative agreement with the experiment. Increasing the microwave amplitude A gives rise to extra current peaks, in addition to the primary single-photon one, corresponding to the successive n -photon resonance $n\hbar\omega = E_2 - E_1$. Here, results up to four-photon transitions are shown [35].

In summary, we studied a p -channel Si MOSFET and identified a spin blockade regime in a double dot system formed by a pair of defects or impurities in the channel. We experimentally observed electrically driven two-spin resonance and found that the spin-orbit interaction suppresses the spin resonance signal near the anticrossing point for both single and multiphoton resonances. Our work shows that impurities or defects in commercial-quality Si MOSFET can be addressed straightforwardly, and they provide a useful window into the electronic spectrum and quantum coherent dynamics. This revelation is particularly appealing when we consider the great practical advantages that the silicon industry could provide to fabricating quantum coherent devices.

We thank M. Kawamura, K. Ishibashi, K. Itoh, S. Kohler, and S. Shevchenko for discussions. This work was supported by JSPS KAKENHI Grant No. 15H04000. This work was partially supported by the RIKEN iTHES Project, the MURI Center for Dynamic Magneto-Optics via the AFOSR Grant No. FA9550-14-1-0040, the Japan Society for the Promotion of Science (KAKENHI), the IMPACT program of JST, CREST, US ARO, and a grant from the John Templeton Foundation.

K. O. and G. G. contributed equally to this work.

*k-ono@riken.jp

- [1] N. C. Jones, R. Van Meter, A. G. Fowler, P. L. McMahon, J. Kim, T. D. Ladd, and Y. Yamamoto, *Phys. Rev. X* **2**, 031007 (2012).
- [2] A. G. Fowler, M. Mariantoni, J. M. Martinis, and A. N. Cleland, *Phys. Rev. A* **86**, 032324 (2012).
- [3] F. Jelezko, T. Gaebel, I. Popa, A. Gruber, and J. Wrachtrup, *Phys. Rev. Lett.* **92**, 076401 (2004).
- [4] A. Morello, C. C. Escott, H. Huebl, L. H. Willems van Beveren, L. C. L. Hollenberg, D. N. Jamieson, A. S. Dzurak, and R. G. Clark, *Phys. Rev. B* **80**, 081307 (2009).
- [5] A. Morello *et al.*, *Nature (London)* **467**, 687 (2010).
- [6] M. Xiao, M. G. House, and H. W. Jiang, *Phys. Rev. Lett.* **104**, 096801 (2010).
- [7] W. F. Koehl, B. B. Buckley, F. J. Heremans, G. Calusine, and D. D. Awschalom, *Nature (London)* **479**, 84 (2011).
- [8] J. J. L. Morton, D. R. McCamey, M. A. Eriksson, and S. A. Lyon, *Nature (London)* **479**, 345 (2011).
- [9] F. A. Zwandenburg, A. S. Dzurak, A. Morello, M. Y. Simmons, L. C. L. Hollenberg, G. Klimeck, S. Rogge, S. N. Coppersmith, and M. A. Eriksson, *Rev. Mod. Phys.* **85**, 961 (2013).
- [10] J. T. Muhonen *et al.*, *Nat. Nanotechnol.* **9**, 986 (2014).
- [11] M. Veldhorst *et al.*, *Nat. Nanotechnol.* **9**, 981 (2014).
- [12] E. Prati, M. Hori, F. Guagliardo, G. Ferrari, and T. Shinada, *Nat. Nanotechnol.* **7**, 443 (2012).
- [13] I. Buluta, S. Ashhab, and F. Nori, *Rep. Prog. Phys.* **74**, 104401 (2011).
- [14] M. F. Gonzalez-Zalba, S. N. Shevchenko, S. Barraud, J. Robert Johansson, A. J. Ferguson, F. Nori, and A. C. Betz, *Nano Lett.* **16**, 1614 (2016).
- [15] C. A. J. Ammerlaan *et al.*, *Impurities and Defects in Group IV Elements and III-V Compounds*, edited by Max Schulz and Landolt-Börnstein, New Series III/22b (Springer, Berlin, 1989).
- [16] A. B. Fowler, G. L. Timp, J. J. Wainer, and R. A. Webb, *Phys. Rev. Lett.* **57**, 138 (1986).
- [17] D. Popović, A. B. Fowler, and S. Washburn, *Phys. Rev. Lett.* **67**, 2870 (1991).
- [18] M. Xiao, I. Martin, E. Yablonovitch, and H. W. Jiang, *Nature (London)* **430**, 435 (2004).
- [19] G. P. Lansbergen, R. Rahman, C. J. Wellard, I. Woo, J. Caro, N. Collaert, S. Biesemans, G. Klimeck, L. C. L. Hollenberg, and S. Rogge, *Nat. Phys.* **4**, 656 (2008).
- [20] K. Y. Tan *et al.*, *Nano Lett.* **10**, 11 (2010).
- [21] M. Pierre, R. Wacquez, X. Jehl, M. Sanquer, M. Vinet, and O. Cueto, *Nat. Nanotechnol.* **5**, 133 (2010).
- [22] M. F. Gonzalez-Zalba, A. Saraiva, M. J. Calderón, D. Heiss, B. Koiller, and A. J. Ferguson, *Nano Lett.* **14**, 5672 (2014).
- [23] K. Ono, T. Tanamoto, and T. Ohguro, *Appl. Phys. Lett.* **103**, 183107 (2013).
- [24] K. C. Nowack, F. H. L. Koppens, Y. V. Nazarov, and L. M. K. Vandersypen, *Science* **318**, 1430 (2007).
- [25] S. Nadj-Perge, S. M. Frolov, E. P. A. M. Bakkers, and L. P. Kouwenhoven, *Nature (London)* **468**, 1084 (2010).
- [26] S. Nadj-Perge, V. S. Pribiag, J. W. G. van den Berg, K. Zuo, S. R. Plissard, E. P. A. M. Bakkers, S. M. Frolov, and L. P. Kouwenhoven, *Phys. Rev. Lett.* **108**, 166801 (2012).
- [27] J. W. G. van den Berg, S. Nadj-Perge, V. S. Pribiag, S. R. Plissard, E. P. A. M. Bakkers, S. M. Frolov, and L. P. Kouwenhoven, *Phys. Rev. Lett.* **110**, 066806 (2013).
- [28] R. Maurand, X. Jehl, D. Kotekar-Patil, A. Corna, H. Bohuslavskyi, R. Laviville, L. Hutin, S. Barraud, M. Vinet, M. Sanquer, and S. De Franceschi, *Nat. Commun.* **7**, 13575 (2016).
- [29] E. Kawakami, P. Scarlino, D. R. Ward, F. R. Braakman, D. E. Savage, M. G. Lagally, M. Friesen, S. N. Coppersmith, M. A. Eriksson, and L. M. K. Vandersypen, *Nat. Nanotechnol.* **9**, 666 (2014).
- [30] K. Takeda *et al.*, *Sci. Adv.* **2**, e1600694 (2016).
- [31] K. Ono, D. G. Austing, Y. Tokura, and S. Tarucha, *Science* **297**, 1313 (2002).
- [32] R. Li, F. E. Hudson, A. S. Dzurak, and A. R. Hamilton, *Nano Lett.* **15**, 7314 (2015).
- [33] H. Bohuslavskyi *et al.*, *Appl. Phys. Lett.* **109**, 193101 (2016).
- [34] J. R. Petta, A. C. Johnson, J. M. Taylor, E. A. Laird, A. Yacoby, M. D. Lukin, C. M. Marcus, M. P. Hanson, and A. C. Gossard, *Science* **309**, 2180 (2005).

- [35] See Supplemental material at <http://link.aps.org/supplemental/10.1103/PhysRevLett.119.156802> for details of experiment and theory, which includes Refs. [36–47].
- [36] G. Giavaras, N. Lambert, and F. Nori, *Phys. Rev. B* **87**, 115416 (2013).
- [37] A. Zarassi, Z. Su, J. Danon, J. Schwenderling, M. Hocevar, B. M. Nguyen, J. Yoo, S. A. Dayeh, and S. M. Frolov, *Phys. Rev. B* **95**, 155416 (2017).
- [38] J. Stehlik, M. Z. Maialle, M. H. Degani, and J. R. Petta, *Phys. Rev. B* **94**, 075307 (2016).
- [39] V. N. Golovach, A. Khaetskii, and D. Loss, *Phys. Rev. B* **77**, 045328 (2008).
- [40] M. Grifoni and P. Hänggi, *Phys. Rep.* **304**, 229 (1998).
- [41] K. Blum, *Density Matrix Theory and Applications* (Springer, Berlin, 2012).
- [42] G. Platero and R. Aguado, *Phys. Rep.* **395**, 1 (2004).
- [43] S. I. Chu and D. A. Telnov, *Phys. Rep.* **390**, 1 (2004).
- [44] S. Kohler, J. Lehmann, and P. Hanggi, *Phys. Rep.* **406**, 379 (2005).
- [45] P. Brune, C. Bruder, and H. Schoeller, *Phys. Rev. B* **56**, 4730 (1997).
- [46] S. J. Chorley, G. Giavaras, J. Wabnig, G. A. C. Jones, C. G. Smith, G. A. D. Briggs, and M. R. Buitelaar, *Phys. Rev. Lett.* **106**, 206801 (2011).
- [47] G. Giavaras (unpublished).
- [48] H. Tezuka, A. R. Stegner, A. M. Tyryshkin, S. Shankar, M. L. W. Thewalt, S. A. Lyon, K. M. Itoh, and M. S. Brandt, *Phys. Rev. B* **81**, 161203(R) (2010).
- [49] J. P. Campbell, P. M. Lenahan, A. T. Krishnan, and S. Krishnan, *J. Appl. Phys.* **103**, 044505 (2008).
- [50] C. P. Slichter, *Principles of Magnetic Resonance* (Springer, Berlin, 1990).
- [51] J. Stehlik, M. D. Schroer, M. Z. Maialle, M. H. Degani, and J. R. Petta, *Phys. Rev. Lett.* **112**, 227601 (2014).
- [52] P. Scarlino, E. Kawakami, D. R. Ward, D. E. Savage, M. G. Lagally, M. Friesen, S. N. Coppersmith, M. A. Eriksson, and L. M. K. Vandersypen, *Phys. Rev. Lett.* **115**, 106802 (2015).